Supplement of Earth Syst. Dynam., 15, 307–322, 2024
https://doi.org/10.5194/esd-15-307-2024-supplement

Earth System Dynamics
Open Access

Supplement of

Solar radiation modification challenges decarbonization with renewable solar energy

Susanne Baur et al.

Correspondence to: Susanne Baur (susanne.baur@cerfacs.fr)

Table S1: Constants and variables used for calculation of PV and CSP potential.

Symbol	Description	Value	Reference
$RSDS$	Downwelling shortwave radiation on horizontal plane	[W m-2]	model output
$RSDS_{diff}$	Downwelling diffuse shortwave radiation	[W m-2]	model output
$RSDS_{dir}$	Downwelling direct shortwave radiation	[W m-2]	Smith et al., 2017
$RSDS_{panel}$	Shortwave radiation on tilted panel	[W m-2]	Smith et al., 2017
h	Hours in a year	8670 [h]	-
A	Suitability factor	0-1	-
a	Area of grid cell	[m2]	-
n_{LPV}	PV land use factor	47 %	Köberle et al., 2015; Ong et al., 2013
n_{LCSP}	CSP land use factor	37 %	Köberle et al., 2015; Trieb et al., 2009
n_{PV}	PV panel efficiency corrected for atmospheric variables	-	-
n_{Panel}	PV panel efficiency under STC	26.8 %	Fraunhofer ISE, 2023; NREL, 2023
n_{CSP}	CSP efficiency corrected for atmospheric variables	-	-
T_p	PV panel temperature	[°C]	-
T	Surface air temperature	[°C]	model output
T_{STC}	PV panel temperature under STC	25 [°C]	Crook et al., 2011
T_f	Fluid temperature in the absorber	115 °C	Dudley 1995; Crook et al., 2011; Dutta et al., 2022; Wild et al., 2017; Gernaat et al., 2021
c_1		4.3 [°C]	Crook et al., 2011; Dutta et al., 2022; Gernaat et al., 2021
c_2		0.943	Crook et al., 2011; Dutta et al., 2022; Gernaat et al., 2021
c_3		0.028 [°C m2 W-1]	Crook et al., 2011; Dutta et al., 2022; Gernaat et al., 2021
c_4		-1.528 [°Csm-1]	Crook et al., 2011; Dutta et al., 2022; Gernaat et al., 2021
V	Surface wind velocity	[ms-1]	model output
PR	Performance ratio	85 %	Fraunhofer ISE, 2023
γ	Efficiency response of mono-silicone PV panels	-0.005 [°C-1]	Dutta et al., 2022; Jerez et al., 2015; Sawadogo et al., 2021; Feron et al., 2021
n_R	Rankine cycle efficiency	40 %	Gernaat et al., 2021
FLH	Full Load Hours	h	-
k_0	-	0.762	Crook et al., 2011; Dudley 1995; Wild et al., 2017; Dutta et al., 2022; Gernaat et al., 2021
k_1	-	0.2125 [W m−2 °C−1]	Crook et al., 2011; Dudley 1995; Wild et al., 2017; Dutta et al., 2022; Gernaat et al., 2021
θ_z	Solar zenith angle	rad	-
α	Solar azimuth angle	rad	-
β	Panel inclination	rad	-

Table S2: Land use suitability fractions assigned to land use cover categories from IMAGE3.0-LPJ (Doelman et al., 2018; Stehfest et al., 2014).

Land use / land cover category	Reference suitability value for PV & CSP
Agricultural land	1 %
Extensive grassland	5 %
Carbon plantation	0
Regrowth forest abandoning	0
Regrowth forest timber	0
Biofuels	0
Ice	0
Tundra	10 %
Wooded tundra	0
Boreal forest	0
Cool conifer forest	0
Temp. mixed forest	0
Temp decid. forest	0
Warm mixed forest	0
Grassland / steppe	10 %
Hot desert	25 %
Scrubland	10 %
Savannah	8 %
Tropical woodland	0
Tropical forest	0

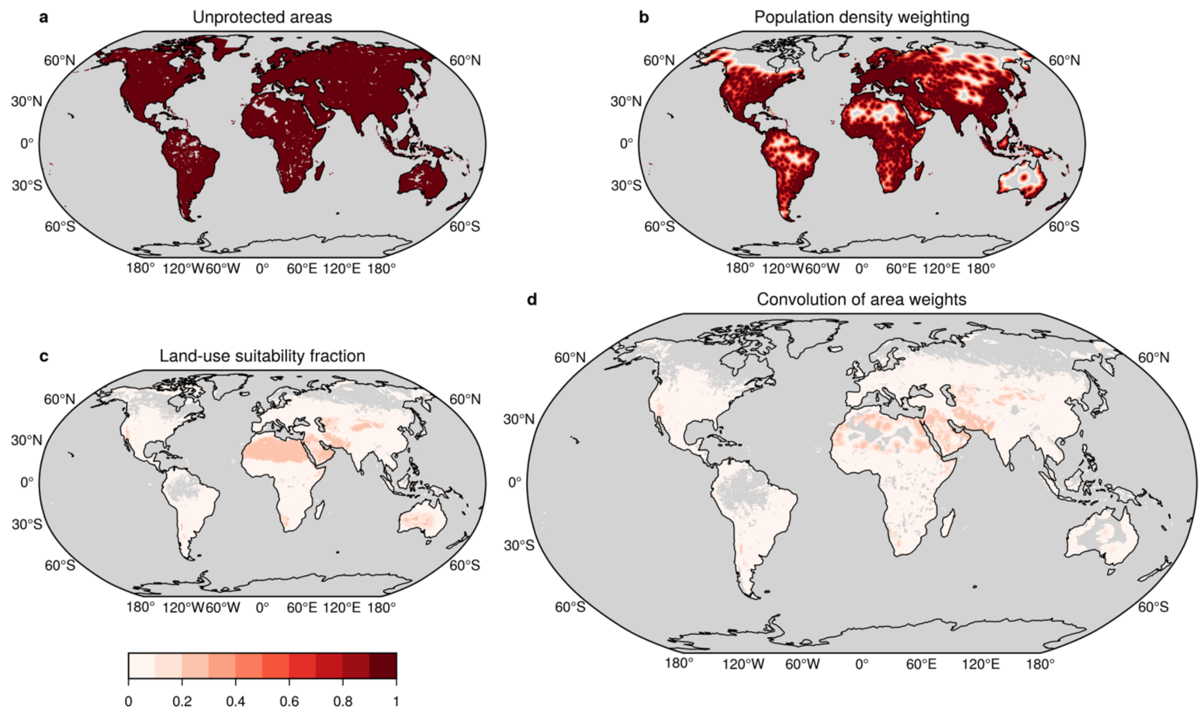

Figure S1: Conceptual figure of the single weights used for area weighting of the technical potential. a) unprotected areas (IUCN), b) weighting of distance to densely populated areas (Stehfest et al., 2014; Doelman et al., 2018), c) weighting according to land use cover (Stehfest et al., 2014; Doelman et al., 2018) and d) convolution of a, b and c.

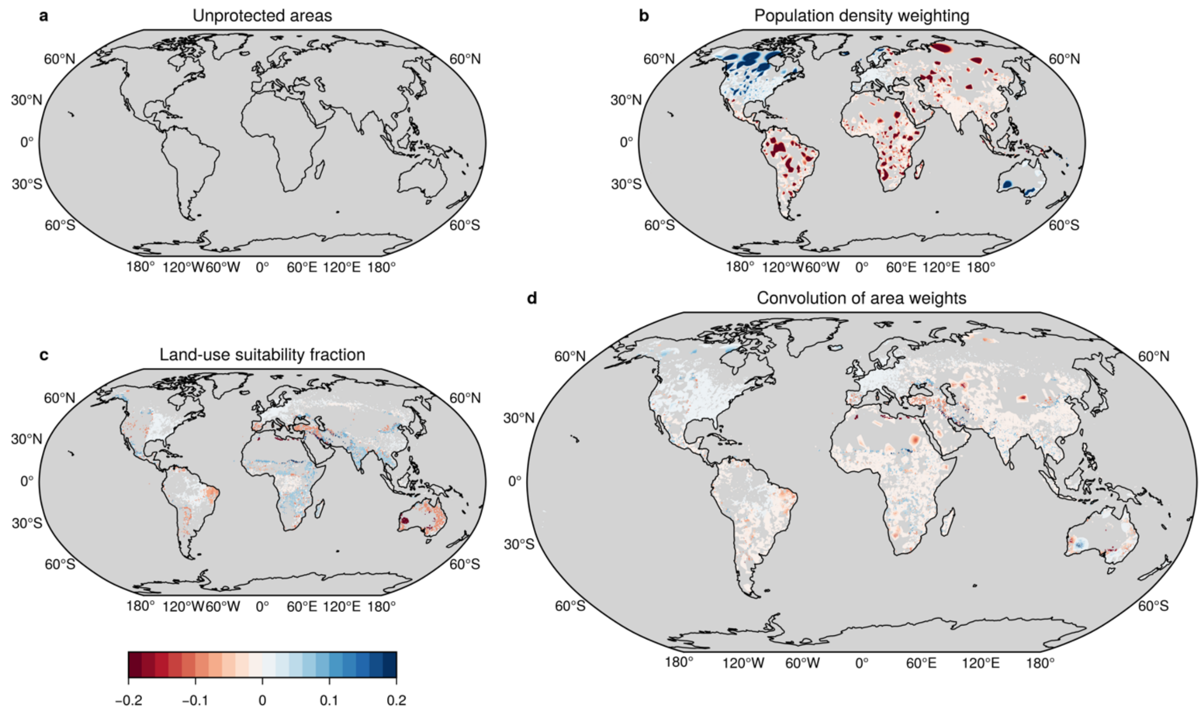

Figure S2: Difference in area weighting between SSP245 and SSP585 for a) unprotected areas (IUCN), b) weighting of distance to densely populated areas (Stehfest et al., 2014; Doelman et al., 2018), c) weighting according to land use cover (Stehfest et al., 2014; Doelman et al., 2018) and d) convolution of a, b and c.

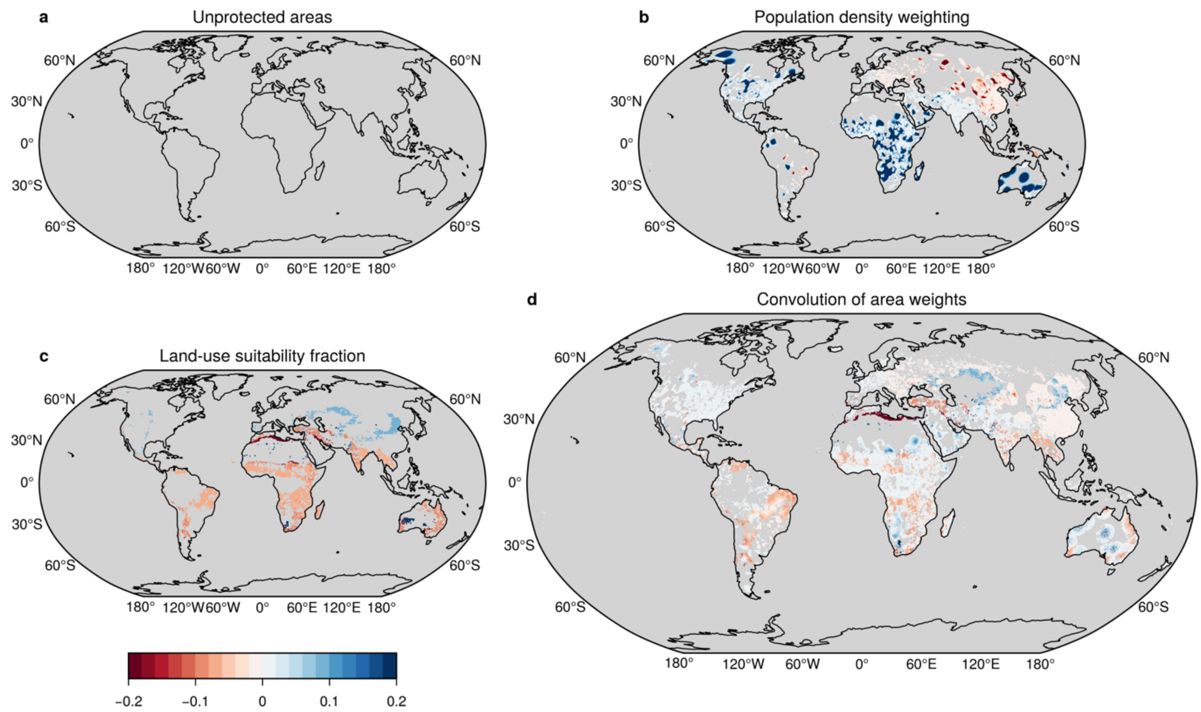

Figure S3: Difference in SSP2 area weighting between the present (2015-2024) and the future (2090-99) for a) unprotected areas (IUCN), b) weighting of distance to densely populated areas (Stehfest et al., 2014; Doelman et al., 2018), c) weighting according to land use cover (Stehfest et al., 2014; Doelman et al., 2018) and d) convolution of a, b and c.

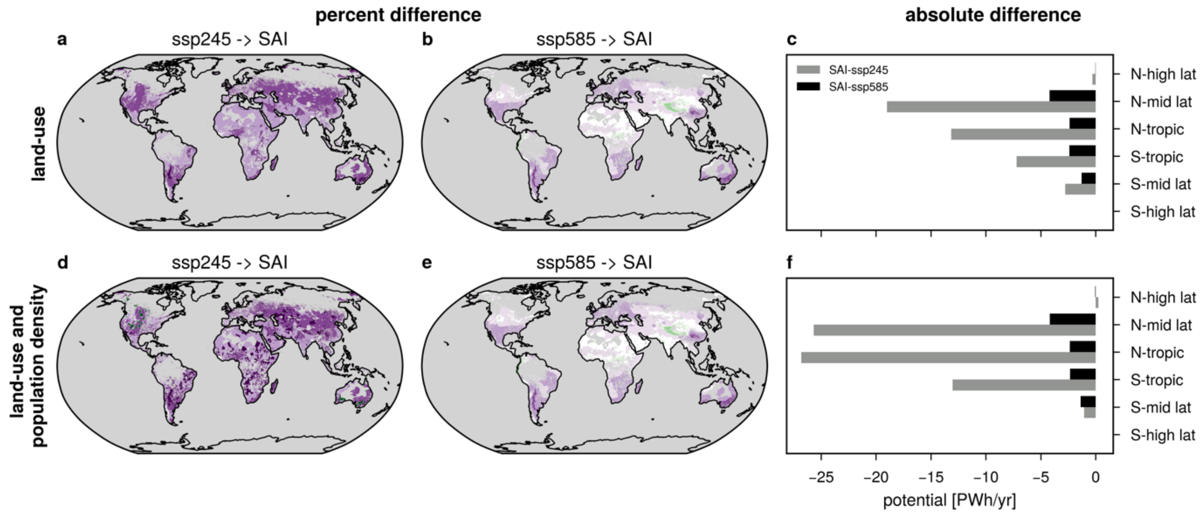

Figure S4: Same as Figure 2 but with a-c) land-use suitability factors and d-f) land-use suitability factors and population density assumptions according to scenario (SSP2 for SSP245; SSP5 for SSP585 and SAI). For a) and d) relative differences are constrained to areas considered suitable under SSP245. Areas that are relevant under SAI but not SSP245 are therefore not displayed. x -> y denotes (y – x)/x.

Table S3: Total global CSP technical potential per scenario in PWh/yr under different geographical constraints but always with the minimum-radiation-requirement constraint.

Geographical constraints	SAI	SSP585	SSP245
Land areas	1,026	1,705	1,679
Unprotected areas on land	859	1,449	1,430
Unprotected areas on land weighted with suitability fractions	126	163	163
Unprotected areas on land weighted with suitability fractions and distance to highly populated areas	73	99	99

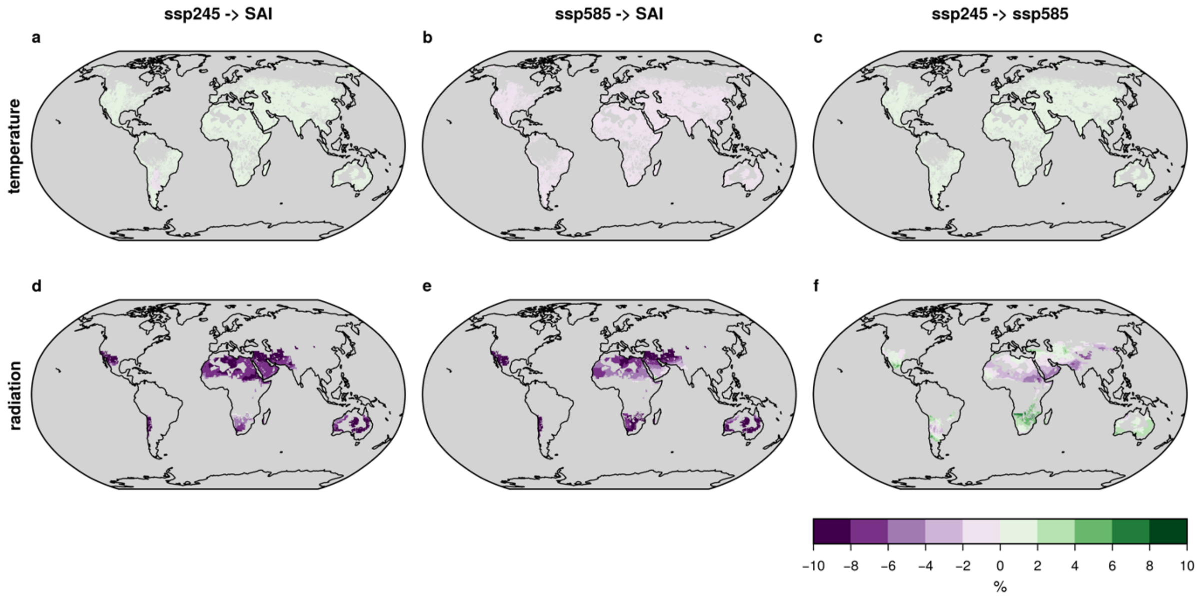

Figure S5: Main drivers of change in 2090-2099 CSP potential, a,b,c) surface air temperature and d-f) total downwelling direct surface radiation. Areas with SNR < 1 are shown in white. x -> y denotes (y – x)/x.

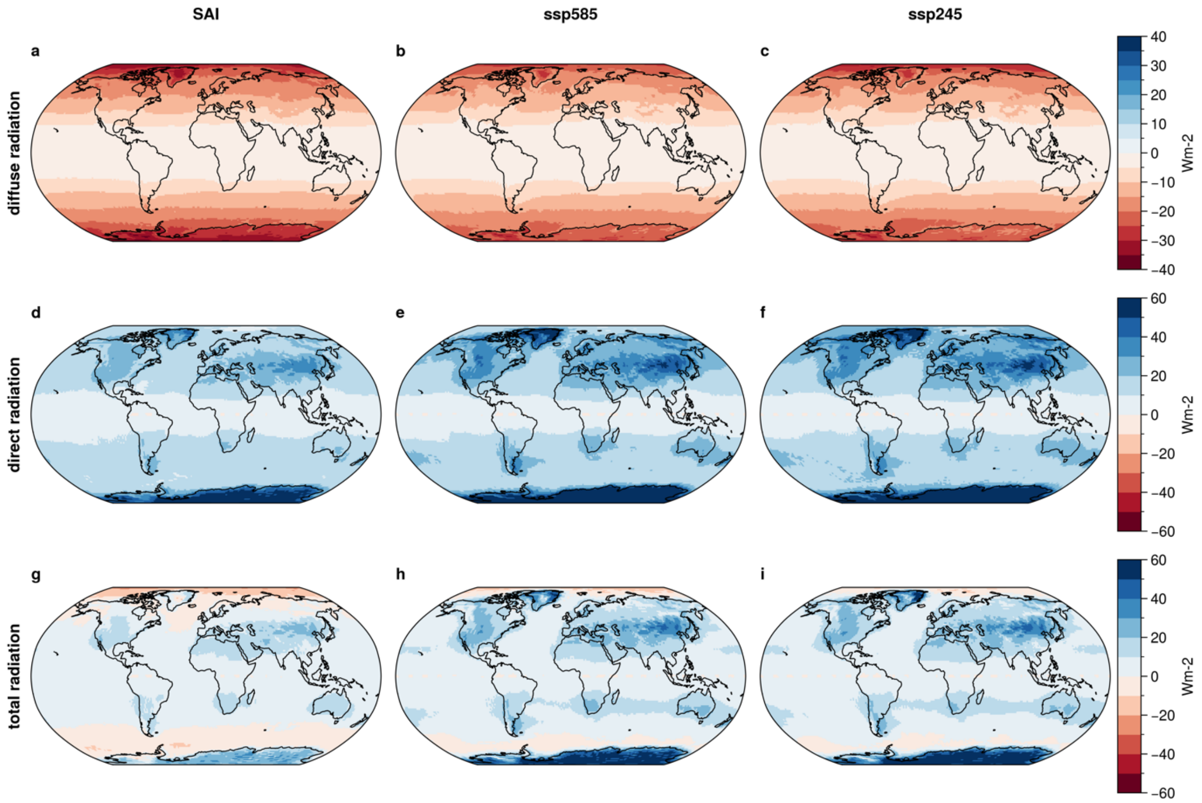

Figure S6: Difference in the direct and diffuse components of the PV potential calculation when solar geometry and panel tilt are accounted for ($RSDS_{panel}$) versus when radiation on a horizontally aligned panel is considered (RSDS). a-c) display the difference in diffuse radiation that is used in $RSDS_{panel}$ versus in RSDS. d-f) same as a-c but for direct radiation. g-j) displays $RSDS_{panel}$ - RSDS.

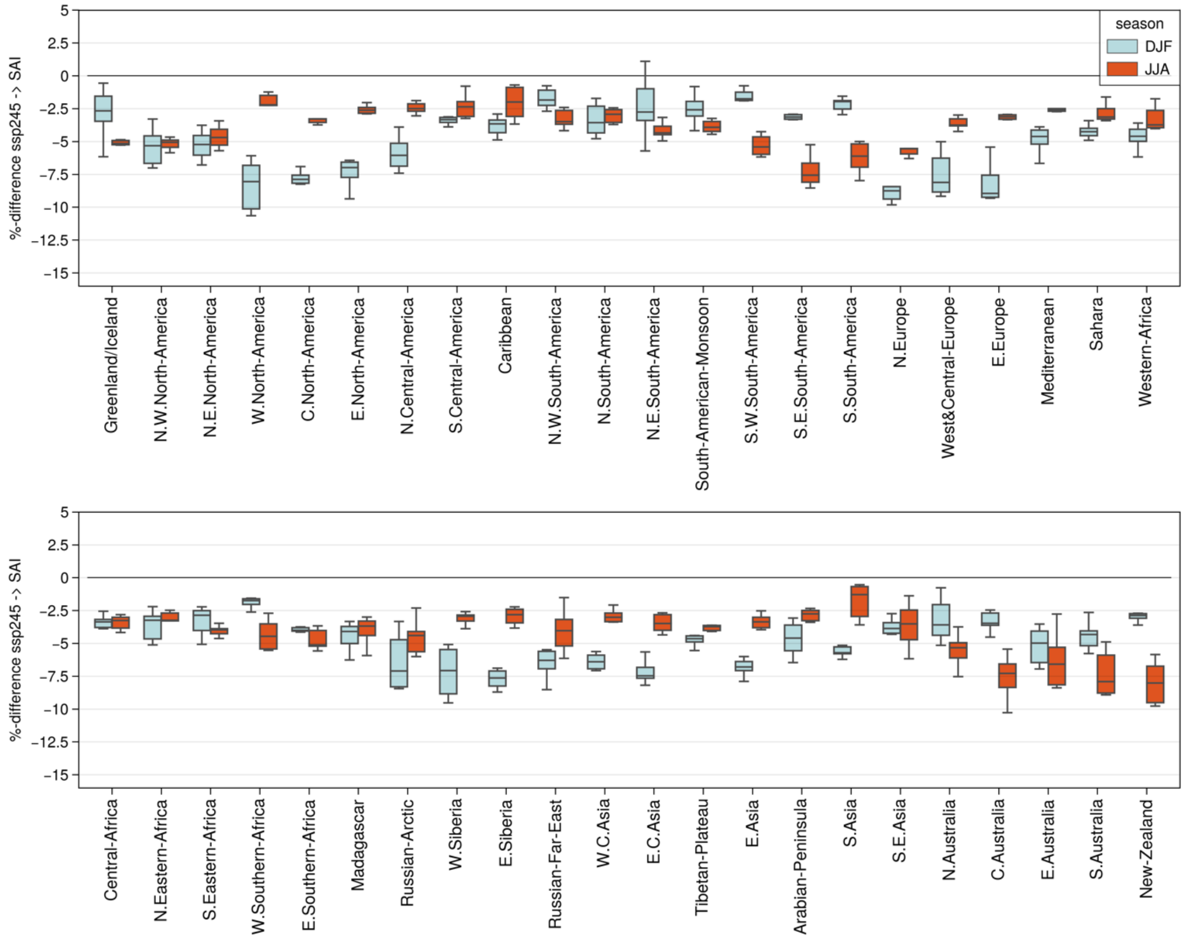

Figure S7: Relative change in 2090-99 PV potential from SSP245 to SAI for all IPCC AR6 regions except Antarctica (Iturbide et al., 2020) split up into two seasons of December, January, February (lightblue) and June, July, August (orangered). Range over boxplot represents the spread over the 6 ensemble members. x -> y denotes (y – x)/x.

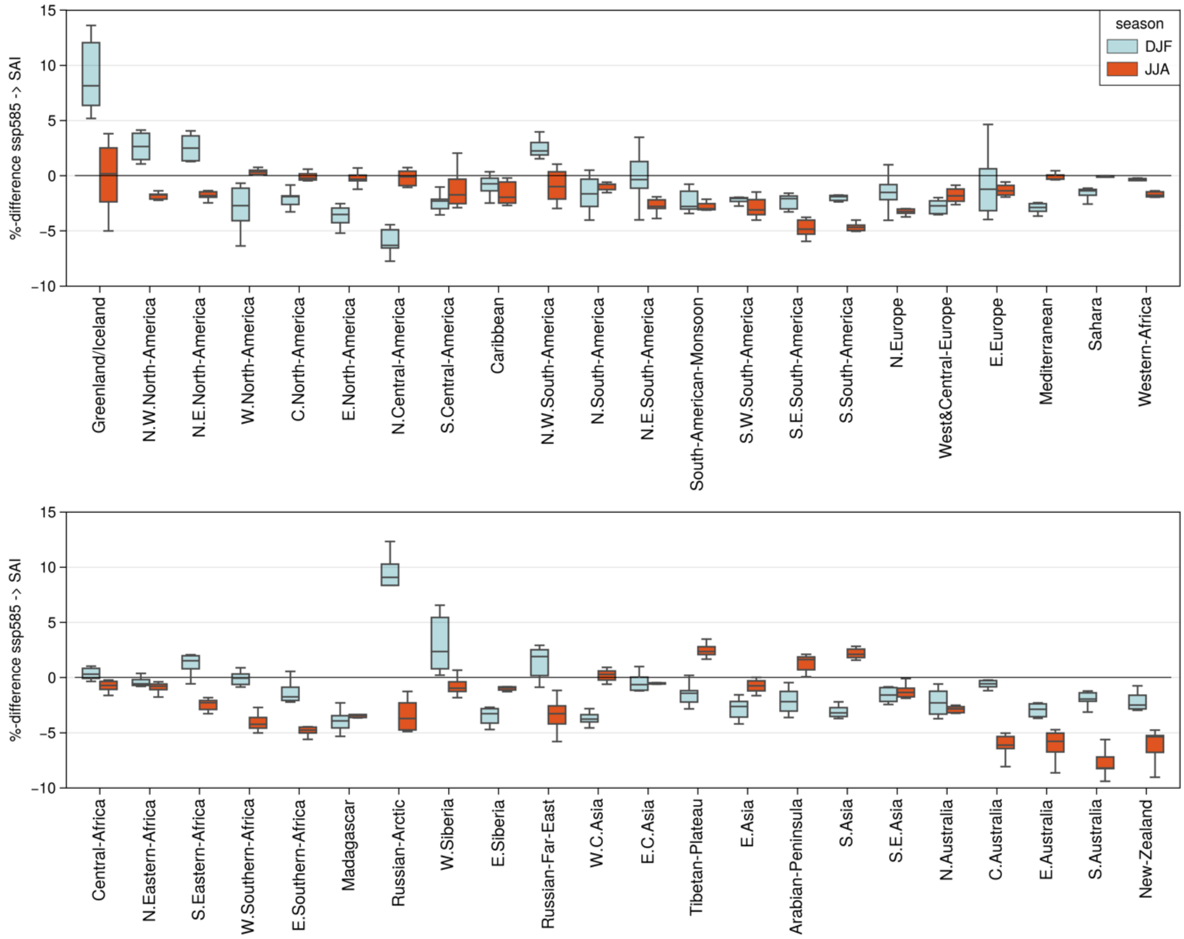

Figure S8: Same as Fig. S7 but for SSP585 -> SAI.

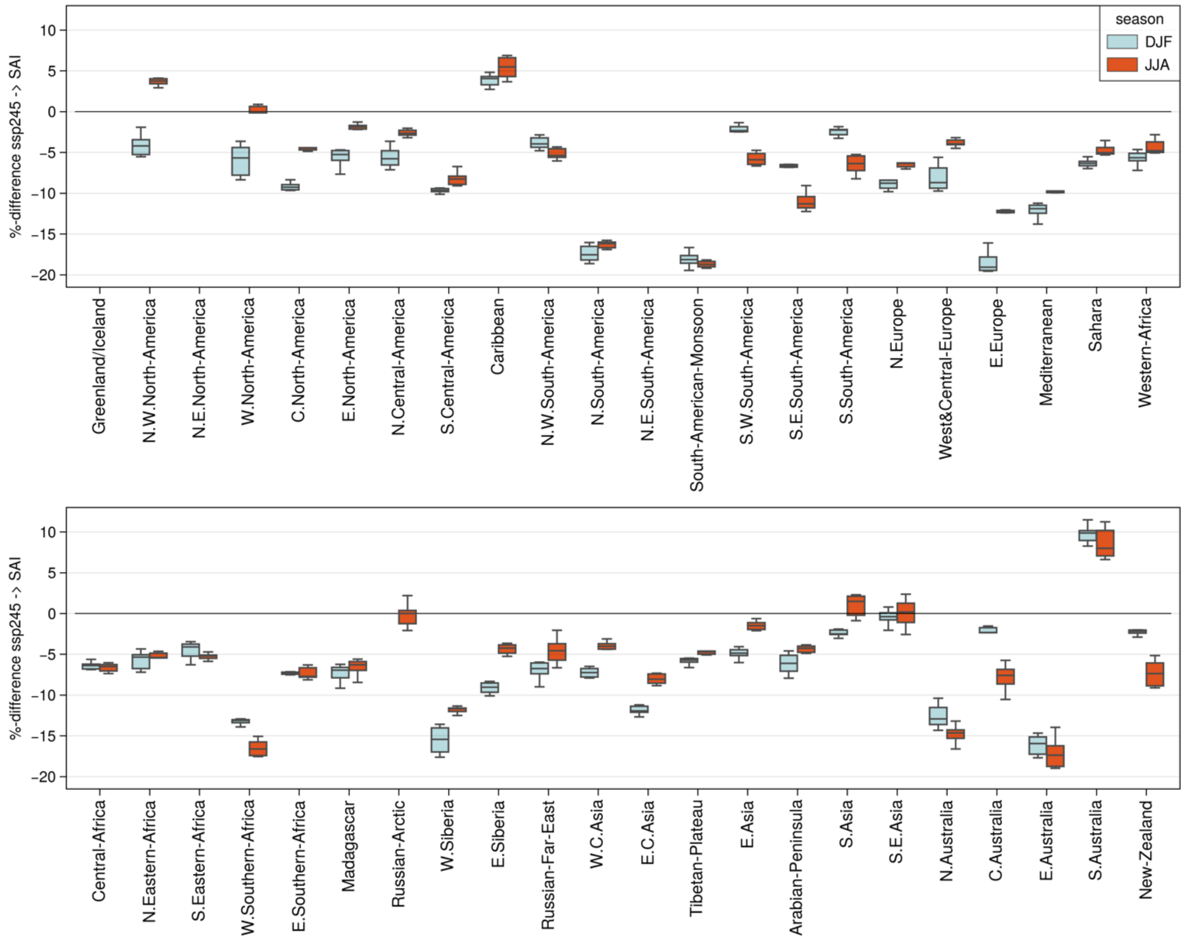

Figure S9: Same as Fig. S7 but with land-use suitability factors and population density according to scenario (SSP2 for ssp245; SSP5 for SAI).

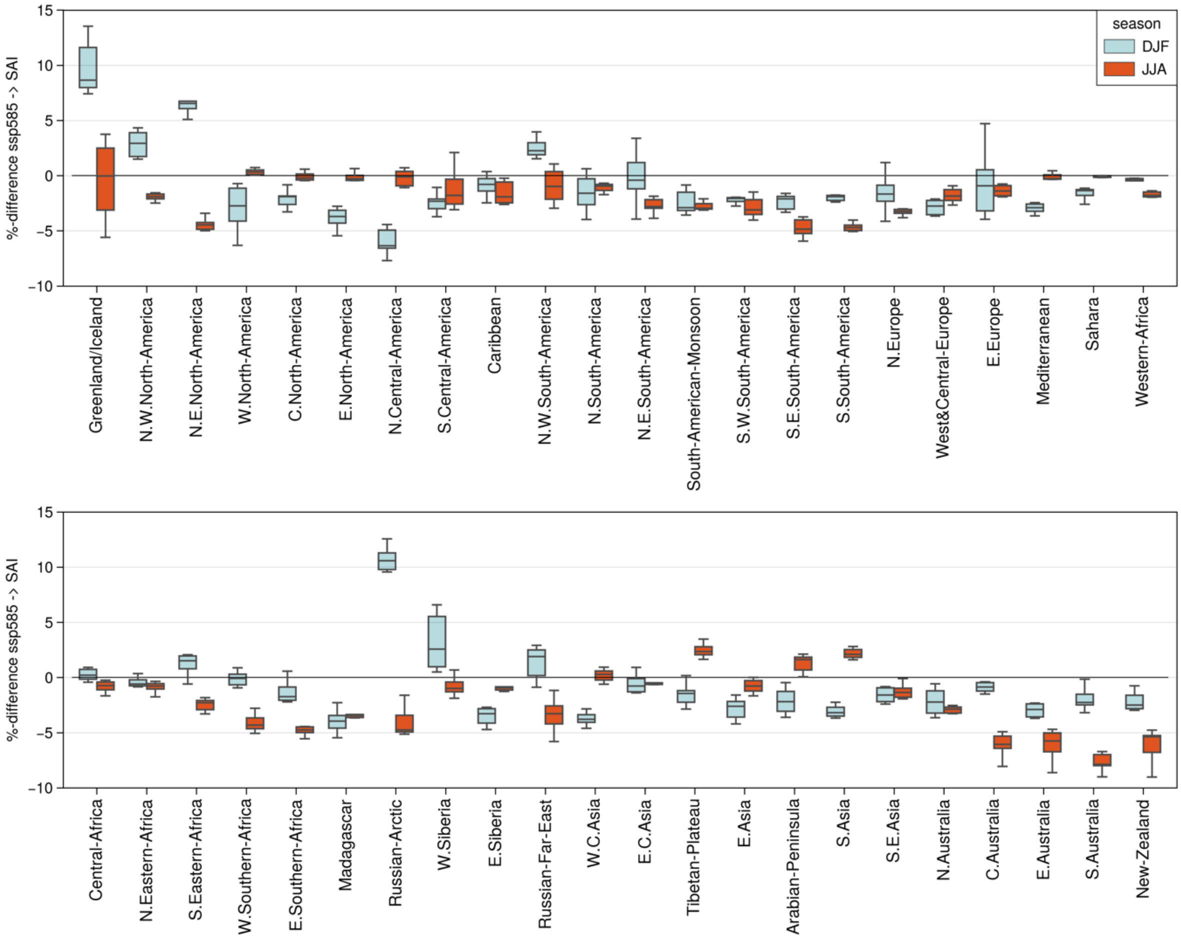

Figure S10: Same as Fig. S7 but for SSP585 -> SAI and with land-use suitability factors and population density according to scenario (SSP5 for ssp585 and SAI).

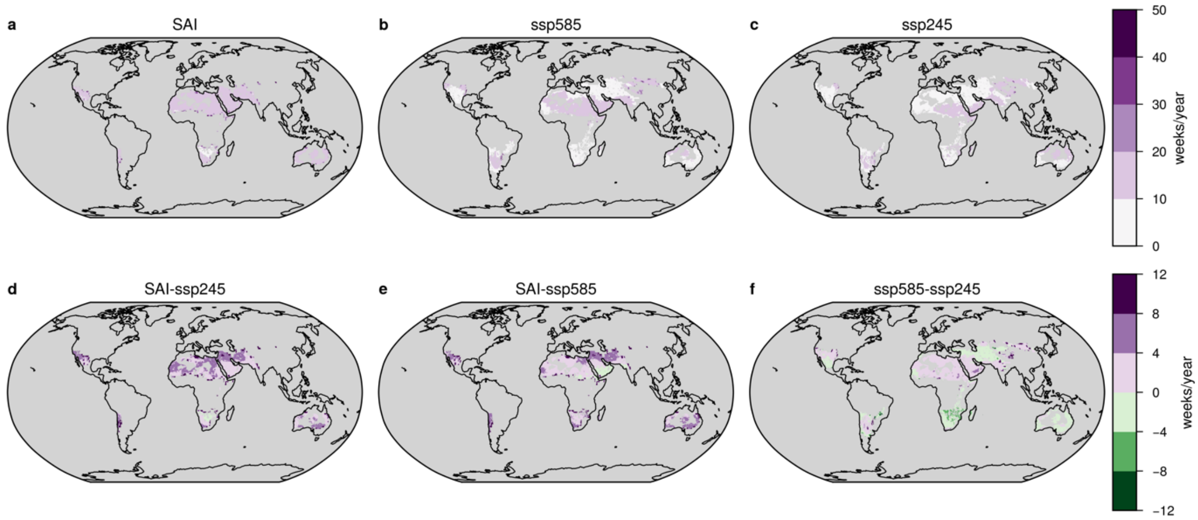

Figure S11: CSP Low Energy Week metric for a) SAI, b) ssp585 and c) ssp245. The LEW is calculated between the present (2015-2019) and the future (2095-2099) with equal area weighting. See 2.3 for the LEW equation.

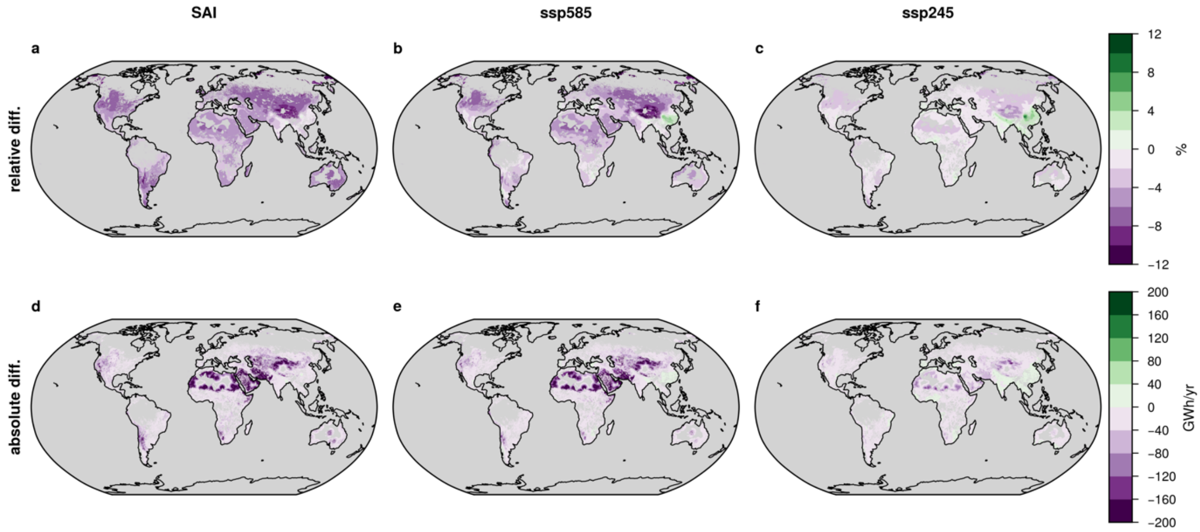

Figure S12: Comparing present (2015-2024) versus future (2090-2099) in relative (a-c) and absolute (d-f) terms for SAI (a,d), ssp585 (b,e) and ssp245 (c,f) using constant area weighting.

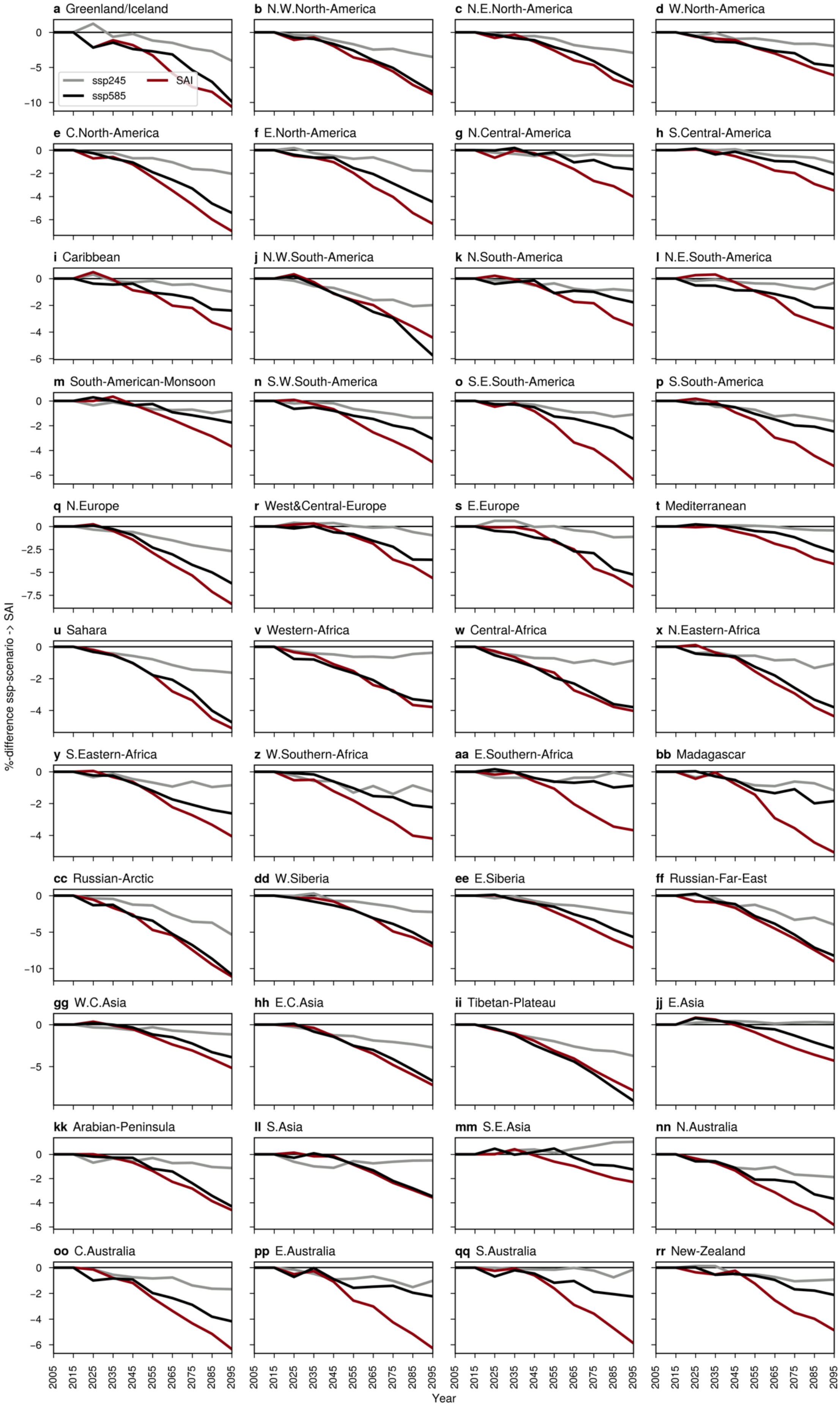
a Greenland/Iceland
b N.W.North-America
c N.E.North-America
d W.North-America
e C.North-America
f E.North-America
g N.Central-America
h S.Central-America
i Caribbean
j N.W.South-America
k N.South-America
l N.E.South-America
m South-American-Monsoon
n S.W.South-America
o S.E.South-America
p S.South-America
q N.Europe
r West&Central-Europe
s E.Europe
t Mediterranean
u Sahara
v Western-Africa
w Central-Africa
x N.Eastern-Africa
y S.Eastern-Africa
z W.Southern-Africa
aa E.Southern-Africa
bb Madagascar
cc Russian-Arctic
dd W.Siberia
ee E.Siberia
ff Russian-Far-East
gg W.C.Asia
hh E.C.Asia
ii Tibetan-Plateau
jj E.Asia
kk Arabian-Peninsula
ll S.Asia
mm S.E.Asia
nn N.Australia
oo C.Australia
pp E.Australia
qq S.Australia
rr New-Zealand
ssp245
ssp585
SAI
%-difference ssp-scenario -> SAI
Year

Figure S13: Relative difference over time of SAI (red), ssp245 (gray) and ssp585 (black) PV potential compared to 2015-2024 values. Lines are the 6-member ensemble means. x -> y denotes (y – x)/x.

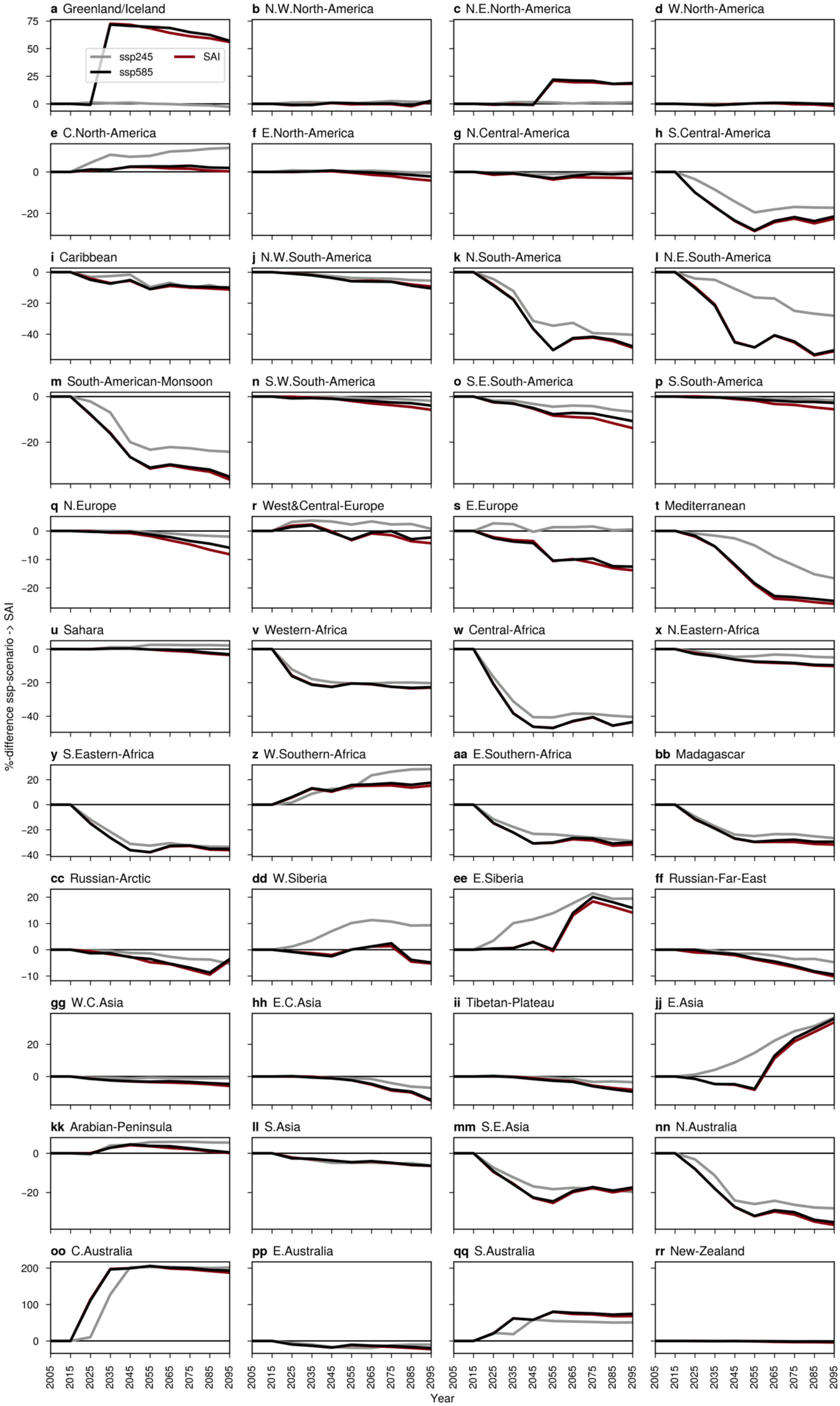
a Greenland/Iceland
b N.W.North-America
c N.E.North-America
d W.North-America
ssp245
ssp585
SAI
e C.North-America
f E.North-America
g N.Central-America
h S.Central-America
i Caribbean
j N.W.South-America
k N.South-America
l N.E.South-America
m South-American-Monsoon
n S.W.South-America
o S.E.South-America
p S.South-America
q N.Europe
r West&Central-Europe
s E.Europe
t Mediterranean
u Sahara
v Western-Africa
w Central-Africa
x N.Eastern-Africa
y S.Eastern-Africa
z W.Southern-Africa
aa E.Southern-Africa
bb Madagascar
cc Russian-Arctic
dd W.Siberia
ee E.Siberia
ff Russian-Far-East
gg W.C.Asia
hh E.C.Asia
ii Tibetan-Plateau
jj E.Asia
kk Arabian-Peninsula
ll S.Asia
mm S.E.Asia
nn N.Australia
oo C.Australia
pp E.Australia
qq S.Australia
rr New-Zealand
%-difference ssp-scenario -> SAI
Year

Figure S14: Relative difference over time of SAI (red), ssp245 (gray) and ssp585 (black) PV potential compared to 2015-2024 values. Land-use suitability weighting according to scenario. Lines are the 6-member ensemble means.

References:

Crook, J. A., Jones, L. A., Forster, P. M., and Crook, R.: Climate change impacts on future photovoltaic and concentrated solar power energy output, Energy and Environmental Science, 4, 3101–3109, https://doi.org/10.1039/c1ee01495a, 2011.

Doelman, J. C., Stehfest, E., Tabeau, A., Van Meijl, H., Lassaletta, L., Gernaat, D. E. H. J., Hermans, K., Harmsen, M., Daioglou, V., Biemans, H., Van Der Sluis, S., and Van Vuuren, D. P.: Exploring SSP land-use dynamics using the IMAGE model: Regional and gridded scenarios of land-use change and land-based climate change mitigation, Global Environmental Change, 48, 119–135, https://doi.org/10.1016/j.gloenvcha.2017.11.014, 2018.

Dudley, V.: SANDIA Report test results for industrial solar technology parabolic trough solar collector, SAND-94-1117, Albuquerque, USA: Sandia National Laboratory, 1995.

Dutta, R., Chanda, K., and Maity, R.: Future of solar energy potential in a changing climate across the world: A CMIP6 multi-model ensemble analysis, Renewable Energy, 188, 819–829, https://doi.org/10.1016/j.renene.2022.02.023, 2022.

Fraunhofer ISE: Photovoltaics report, Fraunhofer Institute for Solar Energy Systems, https://www.ise.fraunhofer.de/content/dam/ise/de/documents/publications/studies/Photovoltaics-Report.pdf, 2023.

Gernaat, D. E. H. J., de Boer, H. S., Daioglou, V., Yalew, S. G., Müller, C., and van Vuuren, D. P.: Climate change impacts on renewable energy supply, Nature Climate Change, 11, 119–125, https://doi.org/10.1038/s41558-020-00949-9, 2021.

Iturbide, M., Gutiérrez, J. M., Alves, L. M., Bedia, J., Cerezo-Mota, R., Cimadevilla, E., Cofiño, A. S., Di Luca, A., Faria, S. H., Gorodetskaya, I. V., Hauser, M., Herrera, S., Hennessy, K., Hewitt, H. T., Jones, R. G., Krakovska, S., Manzanas, R., Martínez-Castro, D., Narisma, G. T., Nurhati, I. S., Pinto, I., Seneviratne, S. I., van den Hurk, B., and Vera, C. S.: An update of IPCC climate reference regions for subcontinental analysis of climate model data: definition and aggregated datasets, Earth System Science Data, 12, 2959–2970, https://doi.org/10.5194/essd-12-2959-2020, 2020.

IUCN (International Union for Conservation of Nature): The World Database on Protected Areas (WDPA), 2023.

Jerez, S., Tobin, I., Vautard, R., Montávez, J. P., López-Romero, J. M., Thais, F., Bartok, B., Christensen, O. B., Colette, A., Déqué, M., Nikulin, G., Kotlarski, S., Van Meijgaard, E., Teichmann, C., and Wild, M.: The impact of climate change on photovoltaic power generation in Europe, Nature Communications, 6, https://doi.org/10.1038/ncomms10014, 2015.

Köberle, A. C., Gernaat, D. E. H. J., and van Vuuren, D. P.: Assessing current and future techno-economic potential of concentrated solar power and photovoltaic electricity generation, Energy, 89, 739–756, https://doi.org/10.1016/j.energy.2015.05.145, 2015.

NREL (National Renewable Energy Laboratory): Best Research-Cell Efficiency Chart, National Renewable Energy Laboratory, https://www.nrel.gov/pv/cell-efficiency.html (last accessed: August 2023), 2023.

Ong, S., Campbell, C., Denholm, P., Margolis, R., and Heath, G.: Land-Use Requirements for Solar Power Plants in the United States, https://doi.org/10.2172/1086349, 2013.

Sawadogo, W., Reboita, M. S., Faye, A., da Rocha, R. P., Odoulami, R. C., Olusegun, C. F., Adeniyi, M. O., Abiodun, B. J., Sylla, M. B., Diallo, I., Coppola, E., and Giorgi, F.: Current and future potential of solar and wind energy over Africa using the RegCM4 CORDEX-CORE ensemble, Clim Dyn, 57, 1647–1672, https://doi.org/10.1007/s00382-020-05377-1, 2021.

Smith, C. J., Crook, J. A., Crook, R., Jackson, L. S., Osprey, S. M., and Forster, P. M.: Impacts of stratospheric sulfate geoengineering on global solar photovoltaic and concentrating solar power resource, Journal of Applied Meteorology and Climatology, 56, 1483–1497, https://doi.org/10.1175/JAMC-D-16-0298.1, 2017.

Stehfest, E., Van Vuuren, D., Kram, T., Bouwman, L., Alkemade, R., Bakkenes, M., Biemans, H., Bouwman, A., Den Elzen, M., Janse, J., Lucas, P., Van Minnen, J., Müller, C., Prins, A.: Integrated Assessment of Global Environmental Change with IMAGE 3.0. Model Description and Policy Applications, Netherlands Environmental Assessment Agency (The Hague), ISBN: 978-94-91506-71-0, 2014.

Trieb, F., Schillings, C., O'Sullivan, M., Pregger, T., and Hoyer-Klick, C.: Global Potential of Concentrating Solar Power, 11, 2009.

Wild, M., Folini, D., and Henschel, F.: Impact of climate change on future concentrated solar power (CSP) production, RADIATION PROCESSES IN THE ATMOSPHERE AND OCEAN (IRS2016): Proceedings of the International Radiation Symposium (IRC/IAMAS), Auckland, New Zealand, 100007, https://doi.org/10.1063/1.4975562, 2017.